Contributed paper

OPTO-ELECTRONICS REVIEW **10**(1), 69–73 (2002)

Tuned liquid crystalline interferometer analysis by means of generalised Berreman matrix

A. WALCZAK*, E. NOWINOWSKI-KRUSZELNICKI, L. JAROSZEWICZ, and P. MARCINIAK

Institute of Applied Physics, Military University of Technology,
2 Kaliskiego Str., 00-908 Warsaw, Poland

The analysis of the tuned, liquid crystalline Fabry-Perot interferometer (FPTI) has been done by means of 4×4 matrix. Wide-angle incidence has been analysed in terms of Trollinger-Chipman correction for extraordinary wave. Results have been applied to determine constraints in design of the monochromatic tuned FPTI. Main features of the FPTI device and liquid crystal determining FPTI parameters has been described in detail. Special attention has been paid to dispersion of the LC' refraction indices as a factor of spectral FPFI' properties.

Keywords: tuned Fabry-Perot interferometer, Berreman matrix, refractive indices, refractive dispersion.

1. Introduction

The free spectral range (FSR) is most important feature of the tuned interferometer. The FSR is a part of FPFI spectrum lying between two adjacent resonance peaks. In liquid crystalline interferometers that part is created by ordinary waves because it is steady versus driving voltage. The extraordinary waves create those resonance peaks, which are voltage tuned over the FSR frequency spectrum. So, it is obvious that as wide as possible FSR is necessary. The range of tuned frequency depends on extraordinary refractive index value. In the liquid crystal (LC) with positive optical anisotropy it is always smaller than FSR. It will be explained that for widest possible spread of tuned frequency the optical anisotropy has to be high, and proper row of the spectrum peak has to be exploited.

The desired feature of FPFI is constant finesse over spread of tuning. Unfortunately, because of dispersion of the refractive indices in LC as well as in mirroring layers it varies over range of tuning.

Those phenomena are always present in liquid crystalline interferometers. So, such devices have to be designed in a little different way than in the classic case.

2. Sample preparation

The Fabry-Perot resonator consists of a pair of commercially available glass plates used in LCD technology covered with 50 nm transparent indium-tin-oxide (ITO) layers. Square sample with clear aperture of 20×20 mm were separated by means of polyimide spacers with diameter near to 0.5 μm. The inner surfaces which form the cavity are flat to $\lambda/20$ at 632.8 nm. Onto these surfaces a multilayer dielectric mirrors have been deposited. On the top of the mirror's surfaces the 20-nm polymide layer have been deposited by spinning method followed by mechanical rubbing. The spectrum of reflectivity of polyimide/mirror/ITO optical buffer has been illustrated in Fig. 1. Glass plates have been assembled using special mount devices and carefully separated with polyimide spacers and screwing to form plane mirror interferometer. Inner cavity has been filled with liquid crystal mixtures by capillary action giving the tilted planar orientation of the layer equivalent to plate with optical axis almost parallel to the surfaces plates. Although the device mount is designed to be thermally stable by careful selection of materials used, in order to maximise the system performance it is still necessary to maintain a thermal control because of the properties of liquid crystal. A separate system keeps the FPF temperature constant to within 0.5°C.

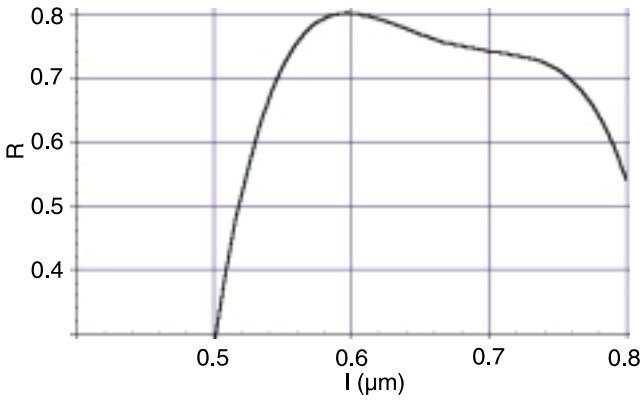

Fig. 1. Reflectivity of the applied optical buffer polyimide/mirror/ /ITO.

*e-mail: awalc@ias.wat.waw.pl

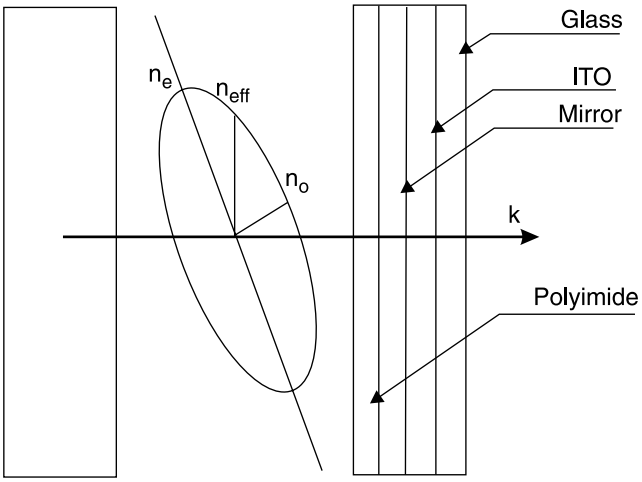

Fig. 2. Scheme of FPF construction.

3. Exploited phenomenon

The FPFI frequency spectrum consists of two different parts. One is dependent on ordinary refractive index of the used LC while the second one is dependent on extraordinary refractive index. In the considered wavelength range dispersion of both indices is present. That dispersion describes the following formula [1]

$$n_{o,e} = A_{o,e} + \frac{B_{o,e}}{\lambda^2} + \frac{C_{o,e}}{\lambda^4}. \tag{1}$$

The coefficients $A_{o,e}$, $B_{o,e}$, $C_{o,e}$ depend on structure of electron bands in LC [1].

The retardation of ordinary and extraordinary waves inside LC layer is different. The phase change $\delta_{o,e}$ is the retardation during dual passage through the LC layer and reflection on both surfaces and is given for ordinary and extraordinary wave, respectively (see Ref. 2 for isotropic case)

$$\frac{\delta_o}{2} = \frac{2\pi d n_o(\lambda)}{\lambda}, \tag{2}$$

$$\frac{\delta_e}{2} = \frac{2\pi d n_e^{eff}(\lambda)}{\lambda}. \tag{3}$$

The coefficients of refraction on the boundary between the LC layer and the optical buffer should be assumed as

$$R = \left(\frac{n_e^{eff}(\lambda) - n_m(\lambda)}{n_e^{eff}(\lambda) - n_m(\lambda)} \right)^2, \tag{4}$$

$$R = \left(\frac{n_o(\lambda) - n_m(\lambda)}{n_o(\lambda) + n_m(\lambda)} \right)^2. \tag{5}$$

The formulae above are for extraordinary and ordinary wave appropriately. Effective refraction index is described by a known formula

$$n_e^{eff} = \frac{n_o n_e}{\sqrt{n_e^2 \sin^2 \varphi + n_o^2 \cos^2 \varphi}}. \tag{6}$$

In Eqs. (4) and (5), n_m denotes coefficient of the optical buffer refraction (see above) which is independently measured. An angle φ is measured between directions of optical axis and the wave vector inside LC layer as it is illustrated in Fig. 2. That formula means that in fact each separate wavelength is reflected with different efficiency. So, real FPF thickness d used in Eqs. (2) and (3) is an effective wave path between points of the wave reflection inside FPFI.

4. Numerical simulations frame

For monochromatic filter application the angular dependence of the spectrum is important. That is the reason to use for FPF simulation a particular method based on Berreman matrix approach. One knows that Berreman matrix eigenvalues are wave vector components along direction perpendicular to the LC layer [4]. So, the procedure for wave vector direction inside LC layer has been added. That procedure exploited Trollinger-Chipman-Wilson method [5] for determining of extraordinary wave vector direction. In that way double check of the results have been achieved.

Berreman proposed the four-dimensional complex vector Ψ_B defined as

$$\overline{\psi} = \begin{pmatrix} E_x \\ H_y \\ E_y \\ -H_x \end{pmatrix} \tag{7}$$

In this vector, the other components of the electromagnetic field are defined as a function of E_x, E_y, H_x, H_y and of the optical properties of medium and of the incidence angle. Expression of the Maxwell equations by mean of Berreman vector result in Berreman equation (see Ref. 4)

$$\frac{d\overline{\psi}(z)}{dz} = i\frac{\varpi}{c} D\overline{\psi}(z), \tag{8}$$

where

$$\Delta = \begin{pmatrix} \Delta_{11} & \Delta_{12} & \Delta_{13} & 0 \\ \Delta_{21} & \Delta_{11} & \Delta_{23} & 0 \\ 0 & 0 & 0 & 1 \\ \Delta_{23} & \Delta_{12} & \Delta_{43} & 0 \end{pmatrix}, \tag{9}$$

and components of it

$$\Delta_{11} = -m\frac{\varepsilon_{xz}}{\varepsilon_{zz}} \quad \Delta_{12} = 1\frac{m^2}{\varepsilon_{zz}} \quad \Delta_{13} = -m\frac{\varepsilon_{yz}}{\varepsilon_{zz}} \tag{10}$$
$$\Delta_{21} = \varepsilon_{xx}\frac{\varepsilon_{xz}^{\ 2}}{\varepsilon_{zz}} \quad \Delta_{23} = \varepsilon_{xy} - \frac{\varepsilon_{xz}\varepsilon_{yz}}{\varepsilon_{zz}} \quad \Delta_{43} = \varepsilon_{yy} - \frac{\varepsilon_{yz}^{\ 2}}{\varepsilon_{zz}} - m^2.$$

The m parameter is given by

$$m = \frac{k_x}{\varpi/c} = n_i \sin\theta_i. \tag{11}$$

where n_i is the external refractive index and θ_i is the incidence angle

As a result, sophisticated description of a normal incidence has been obtained. The consequence is that eigenvalues of the Berreman matrix are ordinary and extraordinary wave vectors values only along direction perpendicular to the illuminated surface. Both vectors lie in the plane of incidence. When optical axis inclination across the LC layer varies rapidly than accuracy of calculations based on Berreman matrix decreases. It is because Berreman matrix is calculated for thin slice of the LC layer with constant inclination of the optical axis. The LC layer was "sliced" in such a way one can assume constant optical inclination in each slice. In the case of very thin LC layer always present in tuned FPF it causes necessity of verification. One is experimental measurement while the second has been used during calculation.

To get mentioned correction during calculations we applied classic description of the wave travelling across LC layer. It has been mentioned that extraordinary wave direction has been obtained by means Trolinger-Chipman-Wilson method. The angle of extraordinary wave refraction is delivered as resolution of the following equation there

$$\vec{k}_e = \vec{k}_i + \vec{\Gamma}, \tag{12}$$

$$\Gamma = \pm\sqrt{\cos^2\varphi_i + (n_i^2 - n_{eff}^2)} - \cos\varphi_i. \tag{13}$$

That formulae has been applied for arbitrary angle of incidence φ_i so, n_i, k_i are the refraction index on the incident wave side and the incident wave vector. Extraordinary wave vector has been denoted as k_e. During calculation all angles are measured from normal incidence direction. Equations (12) and (13) are used in beam propagation method to adjust 4×4-matrix accuracy and to find angular constraints for FPFI designing.

Optical axis inclination has been lead for symmetrically aligned nematic layer in conformity with

$$\varphi(z) = arctg\left[\exp\left(\sqrt{\frac{\varepsilon_o \Delta\varepsilon E^2}{K_F}}\left(z + \frac{d}{2}\right)\right)\right] + \\ + arctg\left[\exp\left(\sqrt{\frac{\varepsilon_o \Delta\varepsilon E^2}{K_F}}\left(-z + \frac{d}{2}\right)\right)\right]. \tag{14}$$

In that model, local value of electric field inside nematic layer has been estimated by $E = U/d$ for U as driving voltage rms and d as layer thickness. After that it has been independently fitted for that model from other measurements [6].

5. Results and discussion

First FPF has been filled with nematic mixture no.1292 from ICH MUT. Measurement of the obtained spectrum proves that proposed theoretical modelling is proper for FPF analysis. We have to underline that repetitive FPF spectrum from one issue to another is loaded by different technological errors. For such a precise device as FPF the errors cause different variations of measured spectra. As that errors are of stochastic character, they are not present in theoretical modelling. Despite this convergence of theoretical and experimental outcomes is good enough to explain what is important in considered FPF designing.

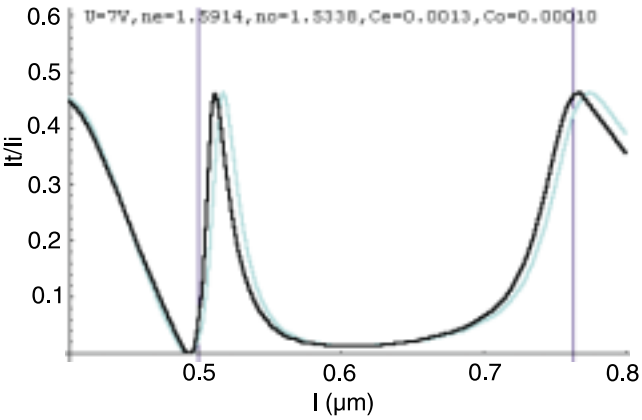

Fig. 3. Results for 1292 mixture filling the FPF cavity (after Ref. 6).

Common use LC such as illustrated no.1292 mixture provides too small spread of tuning. Tuned band range lies between first resonant peaks created by ordinary and extraordinary waves (on the right hand side in Fig. 3). In Fig. 4, tuning process has been exhibited. Conclusion is that relatively small optical anisotropy Δn does not allow obtaining desired FPF parameters. That outcome suggest also that tuned extraordinary resonance peak should not be of the first row.

It may be observed that if LC has properties described by parameters shown in Fig. 4 that FSR is equal to 250 nm while spread of tuning is near to 150 nm. Left-hand side boundary of both bands has been break by spectral edge of the applied mirrors' reflection at about 500 nm (see Fig. 1).

As one can see, optical anisotropy Δn decides about desired range of tuning. The LC with optical anisotropy near to 0.4 must be used to obtain desired result.

If coefficients B_e increases, the characteristic outcome is like in Fig. 5. Enlargement of the C_e coefficient causes

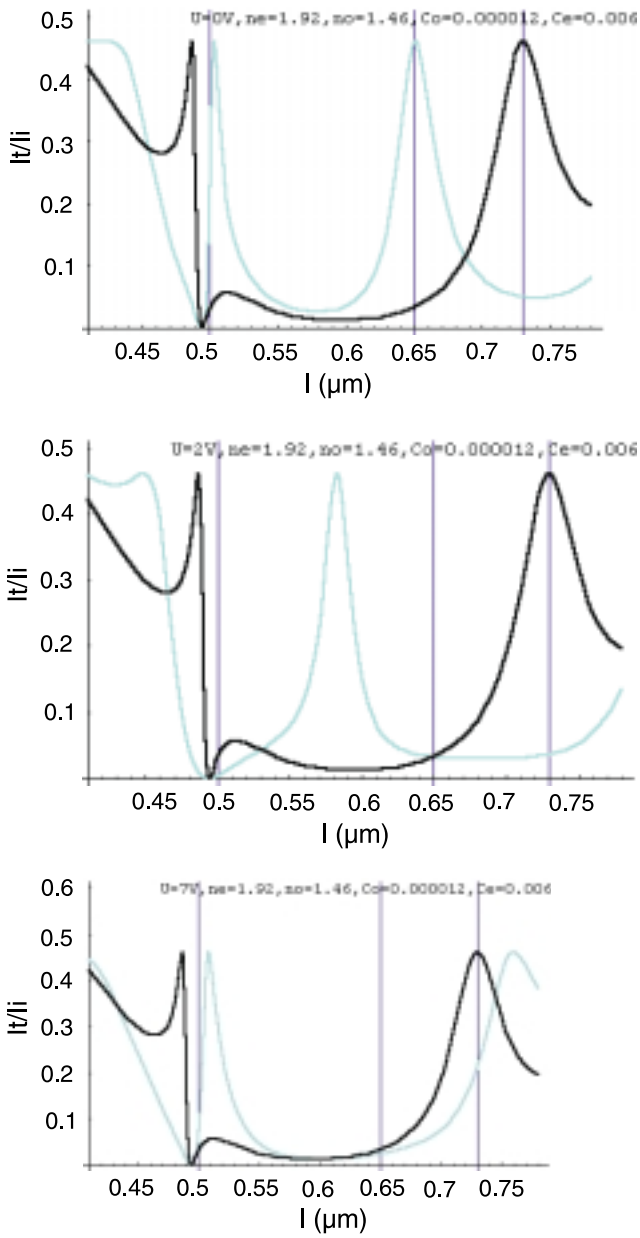

Fig. 4. Movement of the extraordinary resonant peak (grey curve) over FSR created by ordinary resonant peak (black curve) versus driving voltage U. Driving range is from $0V_{rms}$ to $7V_{rms}$. Dispersion of the refractive indices remains unchanged.

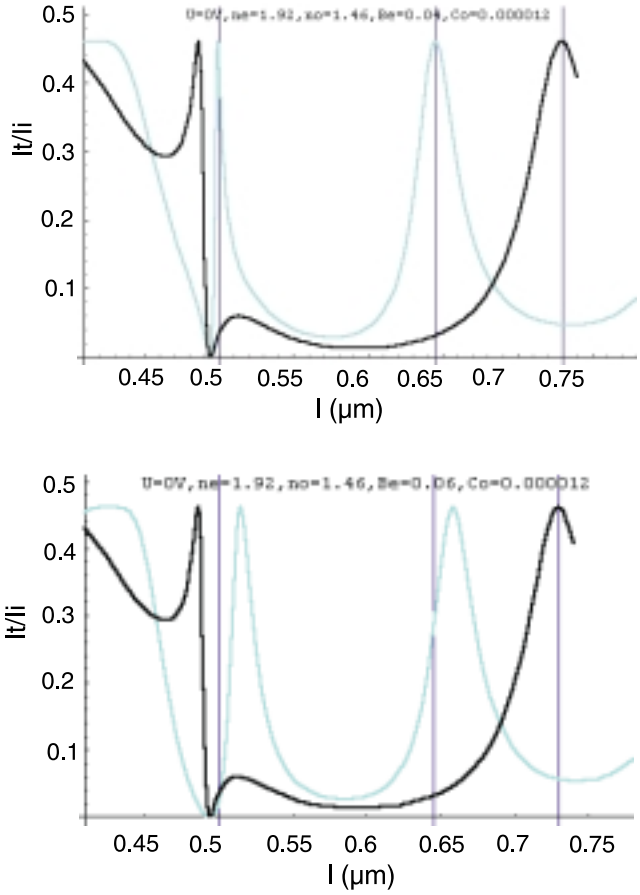

Fig. 5. Dependence of FPFI spectrum on dispersion of extraordinary refraction index.

the same kind situation. It can be observe that such an increase allows make an extension of tuning range. On the other hand, it could destroy monochromatic properties of FPFI because second resonance arise inside FSR range. So, fitting the refractive indices dispersion to improve FPFI parameters have to be done carefully.

6. Conclusions

The aims of the FPF monochromatic filter designing is as wide as possible spread of tuning and, as involved necessity free spectral range (FSR) as well. It has been mentioned that one part of FPFI spectrum is not tuned. It is part joined with ordinary wave inside LC layer. So, resonant peaks of that part stands for FSR. The ordinary refraction index coefficients A_o, B_o, C_o as well as LC layer thickness d have been fitted to assure widest FSR. After that, proper coefficients of extraordinary refraction index have been searched for to give as wide as possible spread of tuning. Calculation has been done by optimisation method.

To obtain highest desired FSR in liquid crystalline FPFI we must use as low ordinary refractive index as possible and row of FPFI ordinary spectrum must be equal to one. The spread of tuning is determined by optical anisotropy. For Δn near to 0.4, one can achieve 150-nm wide spread of tuning. The dispersion of the refractive indices seems to create constraints for monochromatic tuning because it influences the number of separate peak present in the range of tuned frequency. Weak dispersion of extraordinary refractive index is preferred to achieve monochrome, tuned peak inside FSR. Mentioned parameters are basic in designing tuned FPFI with LC layer. Treating results presented above as the start point we do suppose that by applying LC substance with opposite slope then that described above the FSR should be extended.

Acknowledgements

This work is supported by the grant of MUT no. PBW 751 and no. PBS 636.

References

1. I.C. Khoo, S.T. Wu, *Optics and Nonlinear Optics of Liquid Crystals*, World Scientific, Singapore, 1993.
2. H. Haus, *Waves and Fields in Optoelectronics*, Prentice--Hall, London 1984.
3. F. Ratajczyk, *Optics of Anisotropic Centres,* PWN, Warsaw, 1994 (in Polish).
4. D.W. Berreman, "Optics in stratified and anisotropic media: 44-matrix formulation," *J. Opt. Soc. Am.* **62**, 374–1380 (1972).
5. J.D. Trolinger, R.A. Chipman, and D.K. Wilson, "Polarisation ray tracing in birefringent media," *Opt. Eng.* **30**, 461–465 (1991).
6. A. Walczak, "Soliton like solutions and subsurface behaviour of the nematic layer," *Opto-Electron. Rev.* **10**, 43–46 (2002).

Hot off the SPIE Press

Uncooled Thermal Imaging Arrays, Systems, and Applications

by **PaulW. Kruse**, Consultant, Infrared Technology

The development of uncooled infrared focal plane arrays began with the military's need to see the battlefield at night without any form of illumination. The earliest detector arrays required cryogenic cooling. The move to uncooled systems began in the late 1970s and early 1980s with work at Honeywell Technology Center on thin film resistive bolometer arrays and at Texas Instruments on pyroelectric arrays and ferroelectric bolometer arrays. The author worked at Honeywell during the technology's formative period. Like all tutorial texts, this book is intended as an introduction for professionals and students. Topics covered include the principal uncooled thermal detection mechanisms; fundamental performance limits and theoretical performance; the state of the art in uncooled thermal detection; and applications, technical trends, and systems employing uncooled arrays.

Contents: **Overview of un-cooled thermal imaging detection mechanisms and their figures of merit. Fundamental limits. Thermoelectric arrays. Resistive bolometers. Pyroelectric arrays. State of the art technical trends. Choosing the proper technical approach for a given application.**

SPIE PRESS Vol. TT51 • 108 pages
Softcover 0-8194-4122-8 • $35 / $44

Introduction to Laser Diode-Pumped Solid State Lasers

by **Richard Scheps**, Space and Naval Warfare Systems Ctr.

This tutorial text arose from a series of courses presented by the author on laser diode pumping. It covers a wide range of material, from the basics of laser resonators to advanced topics in laser diode pumping. The subject matter is presented in descriptive terms that are understandable by the technical professional who does not have a strong foundation in fundamental laser optics. For the scientist or engineer with a more extensive background in laser design, the range and depth of the topics covered will provide a new and hopefully helpful perspective on development in this highly active area. The book is divided broadly into major sections covering Diode-Pumped Laser Fundamentals; Designing a Diode-Pumped Laser; and Advanced Concepts for Diode Pumping.

SPIE PRESS Vol. 1753
Softcover 0-8194-4274-7 • $35 / $44

Helmet-Mounted Displays: Design Issues for Rotary-Wing Aircraft

by **Clarence E. Rash**, U.S. Army Aeromedical Research Lab.

The rate of incorporation of technology into aviation has been exponential. Advancements in microelectronics, stealth technology, engine design, and electronic sensors and displays have converted simple aircraft into formidable flying machines. In this book, recognized experts in aviation helmet-mounted displays (HMDs) summarize 25 years of knowledge and experience in the area of HMD visual, acoustic, and biodynamic performance, and user interface issues such as sizing, fitting, and emergency egress.

Contents: **Part One-Overview. Image sources. Optical designs. Visual coupling. Part Two-Design Issues. Optical performance. Visual performance. Biodynamics. Acoustical performance. Human factors engineering (HFE) issues. Part Three-HMD Performance Assessment. Test and evaluation. Part Four-Glossary of HMD Terms.**

SPIE PRESS Vol. PM93 • 258 pages
Hardcover 0-8194-3916-9 • $54 / $66

Smart Imaging Systems

Editor: **Bahram Javidi**, Univ. of Connecticut

Imaging systems that were created for military purposes now are available for many commercial applications. Essential to this process is the development of smart imaging devices and systems that integrate sensing, storage, and algorithms. These systems provide new and important capabilities, including highspeed and accurate decision making, large-volume image handling, compactness, and low power consumption. This book presents recent advances in image sensing and processing systems, image recognition, 3D imaging and processing systems, ultrafast optical networks for image communications, and multidimensional information security systems. Students and researchers in information technologies, image processing, and optics will find useful, up-to-date information or current technology. Contributors include leading researchers in the field who provide both theoretical and practical information on recent advances. The text covers image processing and recognition algorithms, 3D sensors and systems, optical storage, and ultrafast optical networks.

Contents: **Analysis of dualband FLIR imagery for automatic target detection. Optimal polarimetric classification of synthetic aperture radar targets. Image security by digital holography. Agile sensing using laserbased systems. Description and applications of a CMOS digital vision chip using general purpose processing elements. Data compression and correlation filtering: a seamless approach to pattern recognition. Recent progress in electro-optical three-dimensional correlators. Robust image recognition in the presence of noise with unknown power. Neural networkbased image preprocessor. Image processing for intelligent transportation systems; application to road sign recognition. Interface between ultrafast optics and optical storage for ultrafast data.**

SPIE PRESS Vol. PM91 • 276 pages
Hardcover 0-8194-3735-2 • $54 / $66

